Water dissociation on the low-coordinated sites of MgO nanopowders

Fabio Finocchi, Francia Haque, Stephane Chenot, Jacques Jupille, Slavica Stankic

Water dissociation on the low-coordinated sites of MgO nanopowders

Fabio Finocchi[#], Francia Haque, Stéphane Chenot, Jacques Jupille and Slavica Stankic[#]

Sorbonne Université, CNRS-UMR 7588, Institut des Nanosciences de Paris
F-75252 Paris Cedex 05, France.
[#]email: fabio.finocchi@sorbonne-universite.fr, slavica.stankic@insp.jussieu.fr

KEYWORDS: oxide, defects, water, adsorption, infrared (IR) spectroscopy, simulations

Abstract

The configurations associated with the dissociative adsorption of water on a variety of low-coordinated sites of MgO(100) surfaces, including corners, steps, MgO vacancies and kinks on <010> steps have been studied and assigned by combining infrared spectroscopy and ab initio *calculations. Three kinds of MgO powders were examined, powders of very high specific surface area prepared by chemical vapor synthesis and well-defined cubic smoke particles obtained by combustion either in 20:80 or 60:40 O_2:Ar mixtures, the latter one involving less defects and smaller particles. It appears that an imperative requirement to obtain a precise characterization of the reactive behavior of defects is to keep the samples in ultra-high vacuum conditions and to control the water partial pressure finely.*

INTRODUCTION

The dissociative adsorption of water molecules on MgO surfaces has been for years a case study. Despite the apparent simplicity of the system, many issues have not been solved yet. The expected full dissociation of isolated water molecules on low-coordinated sites is one of the pending questions. At partial pressure $\leq 10^{-5}$ mbar, water vapor only dissociates on low-coordinated sites of MgO surfaces [1], including steps, corners and vacancies. In such conditions, the hydroxyl coverage determined on the defective (100) face of cleaved crystals was estimated to a few percent [2]. Flat MgO(100) terraces do not dissociate isolated H_2O molecules, even in the case of thin supported films [3] provided they are stoichiometric [4, 5], although at pressures > 10^{-5} mbar the (100) terraces progressively hydroxylate [2, 6, 7]. Consistently, microgravimetric analyses performed on MgO powders obtained by thermal

decomposition of the hydroxide have evidenced a full monolayer OH coverage of the oxide by exposure to saturated vapor pressure at room temperature [8]. The dissociative adsorption of H_2O on monoatomic <010> MgO steps was previously studied by vibrational spectroscopy upon exposure of MgO smoke and MgO films to water vapor [9, 10]. Water splitting at threefold coordinated sites 3C, such as kinks and surface vacancies at monatomic and diatomic steps, has been the object of a theoretical study [Chizallet JACS 2007]. However, little is known on the relative proportion of those sites when the preparation conditions of the powders vary.

The previous findings indicate that a fine analysis of the reactivity of defective MgO surfaces and nano-powders with respect to water vapor imperatively requires ultra-high vacuum (UHV) conditions. Exposure to water vapor at higher pressure than 10^{-5} mbar can indeed induce profound restructuring of the MgO surfaces [6, 12-14] and may cause mass transport [15]. Further, the marginal fraction of the surface occupied by defects suggests to study their hydroxylation on powders by infrared spectroscopy in transmission, in such way that the high specific surface area of the samples should compensate for the scarcity of the sites under study. Two types of powders hold the attention. MgO smokes are collections of cubic nanocrystals that are terminated by (100) facets which involves well-defined <010> steps and exhibit a rather modest surface specific area of the order of 10 m^2g^{-1} [13, 16]. In contrast, a much higher value of ~ 350 m^2g^{-1} characterizes particles that are prepared through chemical vapor synthesis (CVS) [17, 18]. We anticipate that CVS particles, with sizes of a few nanometers, involve a much higher density of low-coordinated sites than smokes. Indeed, the examination of the reactivity of oxide powders in ultra-high vacuum conditions by infrared spectroscopy reveals sites that are not observed by analyses that are commonly operated under high vacuum, as exemplified by the study of hydrogen adsorption on CVS MgO powders [18] and water adsorption on ZnO smokes [19]. As regards the interaction of MgO with water vapor, such study is lacking since, to date, related experiments were only performed in high vacuum conditions [9, 17, 20-21].

The present work aims at exploring the adsorption of water on defective MgO surfaces by infrared spectroscopy (IR) performed in UHV on both smokes and CVS MgO powders. We then compare the vibrational measurements with numerical simulations in order to unravel the contributions of the main

kinds of low-coordinated MgO sites in the hydroxylation process and to determine the nature of the hydroxyl groups.

METHODS

Experiments

Experiments have been performed in an already described UHV apparatus involving a preparation chamber and a main chamber; both with working pressure in the 10^{-10} mbar range [19]. Fourier transform infrared spectroscopy (FTIR) measurements are operated in the main chamber by means of a Bruker Vertex 70 FTIR spectrometer equipped with a MCT detector. Spectra are recorded through ZnSe windows. As starting material to prepare powders, high purity Mg pieces (> 99.98 %) supplied by Goodfellow ™ have been used. MgO smokes have been obtained by burning Mg ribbons within a glove box filled in by dry Ar-O_2 mixtures at the normal pressure. The direct collection of the smoke on a silicon wafer allows for IR analysis in transmission mode since silicon is transparent to IR in the frequency range under study [9, 10]. The CVS-MgO powder was prepared in line with the procedure described in Ref. 16 and pressed into pellets with applied pressure less than five bars to avoid any change in specific surface area. Wafers and pellets were then mounted on a molybdenum plate for insertion and transfer into the UHV apparatus.

The use of MgO smokes raises the question of the exposure of powders to gases in UHV conditions. The purpose of UHV experiments is to keep under control the progressive coverage of initially clean flat surfaces by reactive gases. In a different way, powders are used to obtain sizeable signals. By using, say, CVS powder whose surface specific area is ~ 350 m^2g^{-1}, a MgO pellet of a few tens of milligrams has a total surface area of about 10 m^2, although the area of the pellet itself, of the order of a cm^2, is 10^{-5} lower. In these conditions, the exposure of the whole surface of the material that constitutes the pellet to a gas at a pressure of 10^{-6} mbar would ideally require about a day. Indeed, such estimate is a lower limit that does not take in account nor the diffusion through the pellet nor the reaction of dissociation of the water molecules which would involve a sticking coefficient. An additional concern is the heavy interaction with the reacting gases of some parts of the outer surfaces and the exposure to the residual. Therefore, uncovering the whole surface of a CVS powder in UHV is impossible to achieve in controlled

conditions. The present use of MgO smokes leads to a very different situation. By weighting, we estimated that the deposited smoke covers the supporting wafer with 1 mg per cm^2. Assuming that the specific surface area of the smoke is 10 m^2g^{-1} [13, 16], this corresponds to 100 cm^2 of smoke per cm^2 of wafer. According to the kinetic theory of gas, this means that about 100 seconds are required at the partial pressure of 10^{-6} mbar of water vapor in order to fully expose the smoke sample [13, 16]. As the exposure time is systematically 10 minutes, the surface of the smoke could fully interact with water even at pressures as low as 10^{-7} mbar. The smoke samples offer therefore a reasonable solution to the problem of the analysis of the reactivity of powders in UHV and controlled conditions.

Before being transferred in the main analysis chamber, MgO powders have been degassed at 1170 K in UHV for one hour in the preparation chamber. The applied annealing treatment ensures adsorbate-free MgO surfaces, as confirmed by the absence of any adsorbed impurity in the initial infrared spectrum of the bare MgO powders. We collected reference spectra on the degassed MgO samples in UHV, which we then used for the subtraction. We recorded FTIR spectra with a resolution of 4 cm^{-1} by averaging 250 interferogram scans in order to obtain a reasonable signal-to-noise ratio. The deionized liquid water that was used for adsorption was stored in a reservoir in which it had been purified by freeze-thaw cycles.

Theory

In the following, we focus on water adsorption at low partial pressures (10^{-8}–10^{-5} mbar) or medium pressures (10^{-5}–10^{-3} mbar). At the lowest pressures, all of the previous theoretical investigations agree on the fact that the dissociative adsorption of water on flat MgO(100) terraces only occurs for water clusters and monolayers [23-26], while isolated water molecules adsorbs in a molecular form. In that pressure range, the main contributions to the IR spectra on small MgO nano-powders essentially come from dissociated water at defects [27]. We therefore prepared model surfaces with point defects, such as O vacancies and MgO di-vacancies, as well as mono- and di-atomic steps, either straight or with kinks [18] that spontaneously dissociate a water molecule.

We simulated several adsorption configurations and computed the corresponding O-H vibrations in the OH stretching mode frequency domain via Density Functional Theory (DFT) and Density Functional

Perturbation Theory (DFPT). We carried out the calculations by using the Quantum Espresso program suite [28], within the generalized gradient approximation (PBE) [29]. We accounted for the interaction between the ionic cores and the valence electrons by ultra-soft O, Mg and H pseudopotentials as included in the Quantum Espresso package. We checked that plane-wave cutoffs as large as 40 Ryd on the Kohn-Sham wave functions and four times as large on the electron density and effective potential ensure convergent results. We also chose the k-point sampling, the size of the slab and the void space in order to avoid finite-size effects and obtain unbiased harmonic frequencies.

We then optimized the geometry of all of configurations and determined the corresponding O-H stretching modes via DFPT. In the following, we describe the main characteristics (O-H bond lengths, presence of hydrogen bonds, vibrational frequencies) of the adsorbed hydroxyl groups separately for point defects -- O vacancies, MgO vacancies -- and extended defects -- mono- and di-atomic steps at MgO(100). As the computed harmonic frequencies are slightly overestimated for the isolated water molecule with respect to the experimental values, we rescaled them by a 0.97 factor, thus allowing a better comparison with the measured infrared spectra on hydrated MgO nano-powders. All the reported values for the computed frequencies were rescaled by such a factor.

RESULTS

TEM images and particle size distribution (PSD) diagrams of the three studied MgO samples (20/80, 60/40 and CVS) are shown in Figure 1. CVS MgO powder involves much smaller particles (typical size around 5 nm) than cubic smoke particles that are almost two orders of magnitude larger on average. FTIR transmission experiments have been performed upon exposures at water vapor partial pressures (P_{H20}) ranging between 5×10^{-9} mbar and 1×10^{-5} mbar. On MgO smoke prepared in a 20 % O_2 and 80 % Ar mixture, spectra involve rather sharp bands at 3710-3730 and 3530 cm^{-1}, and broader bands at 3440 and 3220 cm^{-1}, which are all associated to OH stretching frequencies (Figure 2). Moreover, a band at 1635 cm^{-1} is clearly seen at a H_2O partial pressure of 1×10^{-6} mbar and above. On CVS powders, the corresponding frequencies are recorded at 3730-3745, 3550, 3450, 3200-3220 cm^{-1}, while that at 1635 cm^{-1} is hardly observed (Figure 3). Bands recorded on CVS powders are broader (Figure 3) than those collected on smokes (Figure 2), a fact which likely stems from the higher complexity of the surface

provided by the CVS powders. Another important point is the quasi-absence of the band at 1635 cm^{-1}, which unambiguously characterizes molecular water, on the CVS spectra. The abundance of molecular water is consistent with the reactive behavior of powders. At $P_{H20} \geq 10^{-6}$ mbar, the outer parts of the smoke samples are overexposed, which likely favors molecular water adsorption on some highly hydroxylated configurations. Conversely, at $P_{H20} = 10^{-6}$–10^{-5} mbar, the CVS powder is far from being fully hydroxylated and molecular adsorption is marginally observed. More importantly, the observation demonstrates that the bands at 3710-3745, 3530-3550, 3440-3450 and 3200-3220 cm^{-1} are not related to molecular water, but rather to dissociated water molecules.

At pressures ranging between 5×10^{-9} mbar and 10^{-7} mbar, the bands at 3710-3745 cm^{-1} are the unique features that we observed in FTIR spectra recorded on both CVS powders and smokes (Figures 2, 3 and 4). Features at 3530-3550, 3440-3450 and 3200-3220 cm^{-1} appear at $P_{H20} \geq 10^{-6}$ mbar (Figure 4). Recorded at 3730-3745 cm^{-1} on the CVS powder, the highest frequencies on smokes are in the 3710-3730 cm^{-1} range (Figures 2 and 3). Therefore, we carried out measurements on MgO smokes prepared in a 60 % O_2 and 40 % Ar mixture. They consist of MgO smaller nano-cubes than the smokes that were synthesized in the 20 % O_2 and 80 % Ar mixture [30] and are expected to show a higher concentration of low-coordinated sites. Remarkably, the high-frequency band observed after exposing the 60:40 smoke to water at $P_{H20} = 10^{-7}$ mbar is rather close to that found in the CVS spectra (Figure 5).

DISCUSSION

Water dissociation on steps at MgO(100) surfaces is spontaneous, irrespectively of water coverage [27, 31]. This finding can be explained by the higher reactivity of ions with lower coordination number than at flat surfaces (3C at corners and 4C at step edges with respect to 5C on terraces). Another fact driving the dissociation is the reinforcement of the atomic-scale electric field on surfaces such as MgO close to step edges and, even more, at corners [32]. These two factors are linked to each other. As a general and well-documented rule, the stronger the H bond, the longer the ionic-covalent OH bond and the smaller the OH stretching frequencies. This empirical finding is supported by many calculations [11, 33] and can be explained through simple theories of the chemical bond. This is at the root of the interpretation of different values of the OH stretching frequencies ν_{OH}: values around 3700 cm^{-1} are usually referred

to as given by “free OH groups”, meaning that the hydroxyls are not hydrogen bond donors. Smaller values, typically in the range 3400-3600 cm^{-1}, are commonly interpreted as signatures of H-bonded hydroxyls. The smaller values, from 3200 down to 3000 cm^{-1}, have been seldom investigated. In the spectra, they are usually weaker than other signals and, in view of the previous arguments, could correspond to dilated OH bonds because of strong hydrogen bonds. In the following, we will see that there are examples of those abnormally long OH bonds resulting from water dissociation at diatomic steps.

The strategy that we followed to analyze the measurements with the support of the calculations was to focus on the most frequently mentioned sites. They include: (i) three-coordinated corner atoms, $O_{(3C)}$ and $Mg_{(3C)}$ (Figure 6); (ii) monoatomic <010> step with $O_{(4C)}$ and $Mg_{(4C)}$ sites, a type of defect whose occurrence was shown to be very high at the surface of the (100) facets of MgO smokes [8, 11] and (iii) kinks at <010> monoatomic steps with either $O_{(3C)}$ or $Mg_{(3C)}$ corner atoms (Figure 7). All calculated frequencies are shown in Table 1, together with the OH bond lengths and the hydrogen bond lengths. All the configurations that are there presented (Table 1) are calculated to be stable in the pressure range under study.

MgO vacancies on steps and terraces are also included in Table 1. Indeed, they are very reactive towards H_2O and form stable OH complexes on flat MgO(100) terraces [34]. Because of the intense local electric field, MgO vacancies are able to dissociate even the hydrogen molecule with no activation barrier [32]. The reaction of a water molecule with a MgO vacancy at a terrace yields two $O_{(4C)}$-H groups (see Fig.5a) with 0.987 Å bond length, which can be considered as “free” (not hydrogen-bonded). They vibrate around 3460 cm^{-1}. When the MgO vacancy is on monoatomic steps, the reaction produces two $O_{(3C)}$-H groups (see Fig.5b) with 0.971 Å bond length, which vibrate at 3750 cm^{-1}. Neutral oxygen vacancies (F_s centers) can also dissociate water [35, 36] and restore the local ideal stoichiometry. They could also exist in charged states at the surface [37], that is, F_s^+ and F_s^{++}, which are likely stable for highly p-doped MgO. In those cases, the reaction with water is different from the neutral case. However, charged vacancies will not be considered herein.

Involving particles around 5 nm size, CVS powders likely exhibit a relatively high concentration of three-coordinated corner sites. Those sites are expected to react first since they are by far more active

than four-coordinated sites for water dissociation [1]. Close to corners, which we simulate by a kink at a diatomic step, a water molecule can split in two ways: a H-bonded $O_{(1C)}$-H (acceptor) either with $O_{(3C)}$-H or with $O_{(4C)}$-H (donor) groups (Figure 6(a) and 6(b), respectively). In both cases, the $O_{(1C)}$-H (acceptor) has a high stretching frequency (3775 cm^{-1}), while those of the $O_{(3C)}$-H and $O_{(4C)}$-H (donor) hydroxyls are much lower, at about 3090 and 3005 cm^{-1}, respectively (Table1). Interestingly, and somehow against the intuition, $O_{(3C)}$-H groups at corners between diatomic steps also vibrate at rather low frequencies; here, the formation of a strong H bonds with the $O_{(1C)}$-H acceptor is the main factor determining the expansion of the covalent bond and the corresponding stretching mode redshift of the donor hydroxyls. These configurations are associated to the band at 3730-3745 cm^{-1} observed by exposure of the CVS powder to $P_{H20} = 5\times10^{-9}$ - 10^{-7} mbar. As for the calculated bands at 3005-3090 cm^{-1}, that are due to the $O_{(3C)}$-H or $O_{(4C)}$-H (Table 1), they do not clearly appear in the IR spectra. Indeed, the strong H-bonded character of those groups, as indicated by the short H-bond lengths associated to them (Table 1), leads to a very broad band that might be compatible with the faint bump seen in spectra in the 3000-3100 cm^{-1} frequency range (Figure 3).

In the same pressure range (5×10^{-9} - 10^{-7} mbar), the high-frequency bands are slightly red-shifted on the MgO smoke (3710-3730 cm^{-1}, Figs. 2 and 5) with respect to CVS powders. With an average particle size close to 200 nm [16] the proportion of corner sites is very small (for a given volume of powder, the proportion of corner sites goes roughly as the inverse cube of the particle size). Indeed, as steps dominate the defective landscape, vacancies and kinks on steps might provide very reactive 3C sites. Possibilities come from MgO vacancies and kinks on <010> steps. According to calculations, a unique ν_{OH} frequency of 3750 cm^{-1} is associated to the former (Table 1). As kinks are concerned, the $O_{(3C)}$ corner atom is energetically more favorable than the $Mg_{(3C)}$ corner, for the simple reason that two hydroxylated configurations have in common an $O_{(2C)}$-H group bonded to two Mg atoms while the remaining hydroxyl is either $O_{(3C)}$-H, as in Figure 7(b), or $O_{(4C)}$-H, as in Figure 7(c). The water dissociation on $O_{(3C)}$ is predicted to correspond to ν_{OH} frequencies of 3760 and 3735 cm^{-1}. Therefore, MgO vacancies and kinks on mono-atomic steps lead to frequencies in the 3735-3760 cm^{-1} range, thus slightly lower than that at 3775 cm^{-1}, which is associated to corner sites on the CVS sample. The predicted frequencies (3735-3750 cm^{-1}, Table 1) reproduce well the experimental values (3710-3730 cm^{-1} in Figures 2 and 3). The

assignment of the 3710-3730 cm^{-1} band to hydroxyls on kinks at mono-atomic steps is supported by the similarity of the higher frequency recorded on the 60:40 (O_2:Ar) smoke with that of the CVS powder (Figure 5), since the 60:40 (O_2:Ar) smoke likely has less defects and it is closer to stoichiometry than the 20:80 (O_2:Ar) smoke. Moreover, owing to the size of the particles it involves, the 60:40 smoke is expected to exhibit quite many corner sites [30]. Similar ν_{OH} frequencies (3710 and 3750 cm^{-1}) to those found herein (3730-3745 cm^{-1} and 3710-3730 cm^{-1}) were attributed by Knözinger and coworkers to bonded hydroxyls to a $Mg_{(3C)}$ corner and, by comparison to hydrogen adsorption, to a H bonded to an oxygen atom lying at a step edge [17], in full agreement with the configurations described herein.

At straight edges, an isolated water molecule splits into two non-equivalent $O_{(4C)}$-H and $O_{(2C)}$-H hydroxyls. They are tightly H-bonded, as indicated by the quite short H- - - $O_{(2C)}$ bond length (1.88 Å). As a consequence, the covalent bond in the donor $O_{(4C)}$-H group stretches to 0.993 Å, while the computed covalent bond length in the acceptor $O_{(2C)}$-H group is 0.971 Å. At full water coverage, the characteristics of the $O_{(4C)}$-H and $O_{(2C)}$-H groups change with respect to the case of the isolated ones, as the computed bond lengths are 0.984 Å and 0.969 Å, respectively. Especially the $O_{(4C)}$-H bond is impacted, which contracts by ≈ -0.1 Å when passing from the dissociation of the isolated molecule to the full-decorated hydroxyl-covered step. This is due to a progressive weakening of the hydrogen bond between the two hydroxyl groups: the H- - - $O_{(2C)}$ bond passes from 1.88 Å for the isolated dissociated molecule to 2.35 Å at full water coverage. The corresponding stretching frequencies of the $O_{(2C)}$-H groups are around 3750 - 3760 cm^{-1}, depending on the coverage, while those of the H-bond donors $O_{(4C)}$-H vary from 3510 cm^{-1} at full coverage down to 3290 cm^{-1} for the isolated case. In passing, we note that the very important shift of the stretching frequency of the donor hydroxyls with coverage might explain the previous observation of a smaller frequency (3480 cm^{-1}) for the same configuration [9, 10]. When kinks are present at mono-atomic steps, two cases could happen (Figure 7): either the formation of $O_{(3C)}$-H and $O_{(2C)}$-H, which has been retained to partly explain the highest frequency that is observed on smoke, or the formation of $O_{(4C)}$-H and $O_{(2C)}$-H. In the latter case, $O_{(4C)}$-H donates a weak hydrogen bond to $O_{(2C)}$-H; the corresponding stretching frequencies are well distinct (3500 and 3760 cm^{-1}, respectively). The two lower bunches of frequencies that are related to water splitting (either at its onset or at full hydroxyl coverage) on the monoatomic <010> steps and on kinks at those steps, nicely account for the bands at

3530-3550 cm^{-1} and 3200-3220 cm^{-1} that are observed in IR spectra of powders exposed to P_{H20} partial pressures of 10^{-6} - 10^{-5} mbar (Figures 2 and 3). This is also consistent with previous observations that mono-atomic steps are the commonest defects at MgO nano-powders [9]. Finally, dissociative adsorption on MgO vacancies on terraces, with expected ν_{OH} frequency at 3460 cm^{-1} are neither supported nor discarded since the faint feature observed in spectra at that frequency (Figures 2 and 3) already corresponds to several above discussed configurations.

CONCLUSIONS

We have studied water dissociation on low-coordinated sites of MgO in ultra-high vacuum conditions on both, powders prepared by chemical vapor synthesis and smokes. We have exposed the powders to water progressively, starting from partial pressures as low as 5×10^{-9} mbar up to 10^{-5} mbar, in order to avoid the hydroxylation of (100) terraces and eventual mass transport that can occur at higher pressures. We have also faced the problem of exposing a sample of large specific surface area to reactive gases. In this respect, the rather low specific surface area of MgO smokes, which contrasts with the very high specific surface area of CVS powders, offers the possibility to study samples that can be fully exposed at ultra-high vacuum pressures while obtaining an appreciable signal-to-noise ratio in the infrared measurements.

By combining Fourier transform infrared spectroscopy in transmission with *ab initio* calculations, we have identified several significant hydroxyls at corners, mono-atomic <010> steps, kinks and MgO vacancies on mono-atomic steps, which reproduce the experimental outcome qualitatively and quantitatively. This study demonstrates the necessity of experiments performed in ultra-high vacuum conditions on oxide powders in order to understand the reactive behavior of surface defects. This is particularly relevant when, as in the present case for MgO, the oxide is hygroscopic and can undergo deep restructuring after exposure at a pressure beyond a material-specific threshold [14].

REFERENCES

[1] M. A. Henderson: The interaction of water with solid surfaces: fundamental aspects revisited. *Surf. Sci. Rep*. **46** 1 (2002).

[2] P. Liu, T. Kendelewicz, G.E. Brown, G.A. Parks: Reaction of water with MgO(100) surfaces. Part I: Synchrotron X-ray photoemission studies of low-defect surfaces. *Surf. Sci*. **412/413** 315 (1998).

[3] S. Altieri, S. F. Contri, and S. Valeri: Hydrolysis at MgO(100)/Ag(100) oxide-metal interfaces studied by O 1s x-ray photoelectron and Mg $KL_{23}L_{23}$ Auger spectroscopy. *Phys. Rev. B* **76** 205413 (2007).

[4] A.M. Ferrari, S. Casassa, C. Pisani: Electronic structure and morphology of MgO sub-monolayers at the Ag(001) surface: An ab initio model study. *Phys. Rev. B* **71** 155404 (2005).

[5] G. Cabailh, R. Lazzari, J. Jupille, L. Savio, M. Smerieri, A. Orzelli, L. Vattuone, M. Rocca: Stoichiometry-Dependent Chemical Activity of Supported MgO(100) Films. *J. Phys. Chem. A* **115** 7161 (2011).

[6] D. Abriou and J. Jupille: Self-inhibition of water dissociation on magnesium oxide surfaces. *Surf. Sci. Lett*. **430** L527 (1999).

[7] J.T. Newberg, D.E. Starr, S. Yamamoto, S. Kaya, T. Kendelewicz, E.R. Mysak,, O. Soeren Porsgaard, M.B. Salmeron, G.E. Brown Jr., A. Nilsson, H. Bluhm: Autocatalytic Surface Hydroxylation of MgO(100) Terrace Sites Observed under Ambient Conditions. *J. Phys. Chem. C* **115** 12864 (2011).

[8] S. Coluccia, S. Lavagnino, L. Marchese: The hydroxylated surface of MgO powders and the formation of surface sites, *Mater. Chem. Phys*. **18** 445 (1988).

[9] F. Finocchi, R. Hacquart, C. Naud, J. Jupille: Hydroxyl-defect complexes on Hydrated MgO smokes. *J. Phys. Chem. C* **112** 13226 (2008).

[10] L. Savio, M. Smerieri, A. Orzelli, L. Vattuone, M. Rocca, F. Finocchi, J. Jupille: Common fingerprints of hydroxylated non-polar steps on MgO smoke and MgO films. *Surf. Sci*. **604** 252 (2010).

[11] C. Chizallet, G. Costentin, M. Che, F.Delbecq and P. Sautet: Infrared characterization of hydroxyl groups on MgO: A periodic and cluster density functional theory study. *J. Am. Chem. Soc*. **129** 6442 (2007).

[12] C. Duriez, C. Chapon, C.R. Henry, J.M. Rickard: Structural characterization of MgO(100) surfaces. *Surf. Sci*. **230** 123 (1990).

[13] R. Hacquart, J.-M. Krafft, G. Costentin, J. Jupille: Evidence for emission and transfer of energy from excited edge sites of MgO smokes by photoluminescence experiments. *Surf. Sci.* **595** 172 (2005).

[14] M. Ončák, R. Włodarczyk, J. Sauer: Water on the MgO(001) Surface: Surface Reconstruction and Ion Solvation. *J. Phys. Chem. Lett*. **6** 2310 (2015).

[15] D. Thomele, A.R. Gheisi, M. Niedermaier, M.S. Elsässer, J. Bernardi, H. Grönbeck, O. Diwald: Thin water films and particle morphology evolution in nanocrystalline MgO. *J. Am. Ceram. Soc*. **1** (2018). DOI: 10.1111/jace.15775

[16] R. Hacquart, J. Jupille: Morphology of MgO smoke crystallites upon etching in wet environment. *J. Cryst. Growth* **311** 4598 (2009).

[17] E. Knözinger, K.-H. Jacob, S. Singh, P. Hofmann: Hydroxyl groups as IR active surface probes on MgO crystallites. *Surf. Sci*. **290** 388 (1993).

[18] F. Haque, F. Finocchi, S. Chenot, J. Jupille, S. Stankic: Towards a comprehensive understanding of heterolytic splitting of H_2 at MgO surface defects: site reactivity, proximity effects and co-adsorption of several molecules. *J. Phys. Chem. C* **122**, 17738−17747 (2018).

[19] F. Haque, S. Chenot, A F. Viñes, F. Illas, S. Stankic, J. Jupille: ZnO powders as multi-facet single crystals. *Phys. Chem. Chem. Phys*. **19** 10622 (2017).

[20] O. Diwald, M. Sterrer, E. Knözinger: Site selective hydroxylation of the MgO surface. *Phys. Chem. Chem. Phys*. **4** 2811 (2002).

[21] R. Hacquart, J. Jupille: Morphology of MgO smoke crystallites upon etching in wet environment. *J. Cryst. Growth* **311** 4598 (2009).

[22] S. Stankic, A. Sternig, F. Finocchi, J. Bernardi, O. Diwald: Zinc Oxide Scaffolds on MgO Nanocubes. *Nanotechnology* **21** 355603 (2010).

[23] L. Giordano, J. Goniakowski, J. Suzanne: Partial Dissociation of Water Molecules in the (3x2) Water Monolayer Deposited on the MgO (100) Surface. *Phys. Rev. Lett*. **81** 1271 (1998).

[24] M. Odelius: Mixed molecular and dissociative water adsorption on MgO(100). *Phys. Rev. Lett*. **82** 3919 (1998).

[25] L. Delle Site, A. Alavi, R.M. Lynden-Bell: The structure and spectroscopy of monolayers of water on MgO: An ab initio study. *J. Chem. Phys*. **113** 3344 (2000).

[26] R.S. Alvim, I. Borges Jr., D.G. Costa, A.A. Leitao: Density-Functional Theory Simulation of the Dissociative Chemisorption of Water Molecules on the MgO(001) Surface. *J. Phys. Chem. C* **116** 738. (2012).

[27] D. Costa, C. Chizallet, B. Ealet, J. Goniakowski, F. Finocchi: Water on extended and point defects at MgO surfaces. J. Chem. Phys. **125** 054702 (2006).

[28] P. Giannozzi, S. Baroni, N. Bonini, M. Calandra, R. Car, C. Cavazzoni, D. Ceresoli, G.L. Chiarotti, M. Cococcioni, I. Dabo, A. Dal Corso, S. Fabris, G. Fratesi, S. de Gironcoli, R. Gebauer, U. Gerstmann, C. Gougoussis, A. Kokalj, M. Lazzeri, L. Martin-Samos, N. Marzari, F. Mauri, R. Mazzarello, S. Paolini, A. Pasquarello, L. Paulatto, C. Sbraccia, S. Scandolo, G. Sclauzero, A.P. Seitsonen, A. Smogunov, P. Umari, R.M. Wentzcovitch: QUANTUM ESPRESSO: a modular and open-source software project for quantum simulations of materials. *J.Phys.:Condens.Matter* **21** 395502 (2009).

[29] J.P. Perdew, K. Burke, M. Ernzerhof: Generalized-gradient Approximation made simple. *Phys. Rev. Lett*. **77** 3865 (1996).

[30] S. Stankic, M. Cottura, D. Demaille, C. Noguera, J. Jupille: Nucleation and growth concepts applied to a stoichiometric compound formed from a vapor: the case of MgO smoke. *J. Crystal Growth* **329** 52 (2011).

[31] W. Langel, M. Parrinello: Hydrolysis at stepped MgO surfaces. *Phys. Rev. Lett*. **73** 504 (1994).

[32] A. D'Ercole, C. Pisani: *Ab initio* study of hydrogen dissociation at a surface divacancy on the (001) MgO surface. *J. Chem. Phys.* **111** 9743 (1999).

[33] D. Costa and C. Chizallet: Water on extended and point defects at MgO surfaces. *J. of Chem. Phys.* **125**, 054702 (2006).

[34] B. Ealet, J Goniakowski, F. Finocchi: Water dissociation on a defective MgO(100) surface: role of divacancies. *Phys. Rev. B* **69** 195413 (2004).

[35] F. Finocchi, J. Goniakowski: Interaction of a water molecule with the O vacancy on the MgO(100) surface. *Phys. Rev. B* **64** 125426 (2001).

[36] RD. Alvim, I. Borges and AA. Leitao: Proton migration on perfect, vacant and doped MgO (100) surfaces: Role of dissociation residual groups. *J. of Phys. Chem. C* **122** (38) 21841 (2018).

[37] N.A. Richter, S. Sicolo, S.V. Levchenko, J. Sauer, M. Scheffler: Concentration of vacancies at metal-oxide surfaces: case study of MgO(100). *Phys. Rev. Lett*. **111** 045502 (2013).

Table I. Computed characteristics of the hydroxyl groups on several defects at MgO(100) surfaces: O coordination number, OH bond lengths, hydrogen bond lengths and OH stretching frequencies.

Defect	Hydroxyl groups	OH bond lengths (Å)	Hydrogen bond length (Å)	OH stretching frequencies (cm^{-1})
O vacancy @ (100) terrace (F_s center)	No OH groups (vacancy is healed and H_2 released)			
MgO vacancy @ (100) terrace	$O_{(4C)}$-H $O_{(4C)}$-H	0.987 0.987	No H bond	3460 3460
MgO vacancy @ <010> step	$O_{(3C)}$-H $O_{(3C)}$-H	0.971 0.971	No H bond	3750 3750
<010> step (isolated H_2O)	$O_{(2C)}$-H $O_{(4C)}$-H	0.971 0.993	 1.88	3750 3290
<010> step (full H_2O coverage)	$O_{(2C)}$-H $O_{(4C)}$-H	0.969 0.984	 2.35	3760 3510
Kink @ <010> step	$O_{(2C)}$-H $O_{(3C)}$-H	0.970 0.972	No H bond	3750 3735
Kink @ <010> step	$O_{(2C)}$-H $O_{(4C)}$-H	0.968 0.985	 2.25	3760 3500
Corner	$O_{(1C)}$-H $O_{(3C)}$-H	0.967 1.004	 1.70	3775 3090
Corner	$O_{(1C)}$-H $O_{(4C)}$-H	0.967 1.010	 1.74	3775 3005

Figure captions

Figure 1. TEM images and particle size distribution (PSD) diagrams of the three studied MgO samples.

Figure 2. FTIR spectra recorded during exposures of MgO smoke prepared in a 20 % O_2 and 80 % Ar mixture to water vapor at different pressures shown in figure.

Figure 3. FTIR spectra recorded during exposures of CVS powder to water vapor at different pressures shown in figure.

Figure 4. High frequency region of the FTIR spectra shown in Figure 2 (exposures of MgO smoke prepared in a 20 % O_2 and 80 % Ar mixture).

Figure 5. Comparison of the high frequency features that appear at the onset of the exposure to water vapor on, from top to bottom: MgO smoke prepared in a 20 % O_2 and 80 % Ar mixture, CVS powders, MgO smoke prepared in a 60 % O_2 and 40 % Ar mixture

Figure 6. Configurations of a dissociated water molecule at a corner. Top $O_{(1C)}$-H and $O_{(3C)}$-H; bottom: $O_{(1C)}$-H and $O_{(4C)}$-H groups. The corresponding stretching frequencies are reported.

Figure 7. Configurations of a dissociated water molecule at a mono-atomic <010> step. From top to bottom: straight step with $O_{(2C)}$-H and $O_{(4C)}$-H groups, kink with $O_{(2C)}$-H and $O_{(3C)}$-H or $O_{(2C)}$-H and $O_{(4C)}$-H groups. The corresponding stretching frequencies are reported.

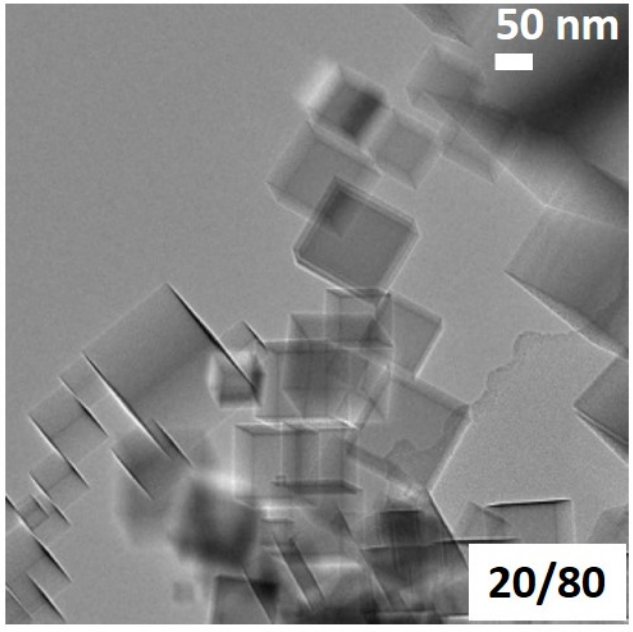
50 nm
20/80

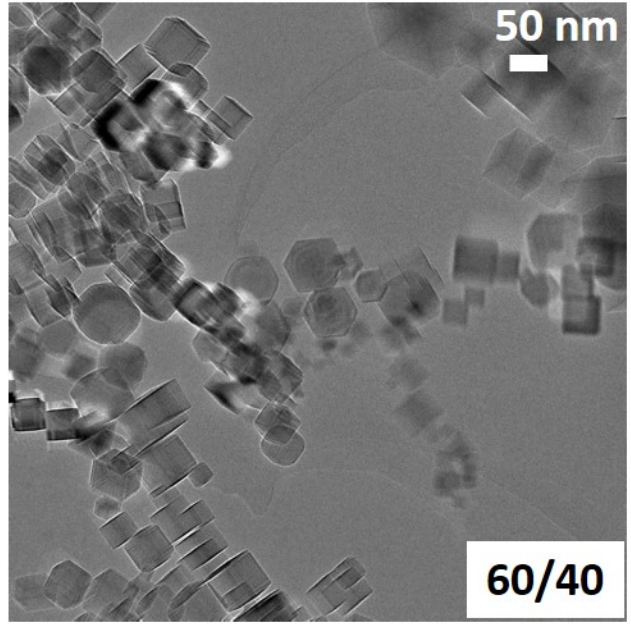
50 nm
60/40

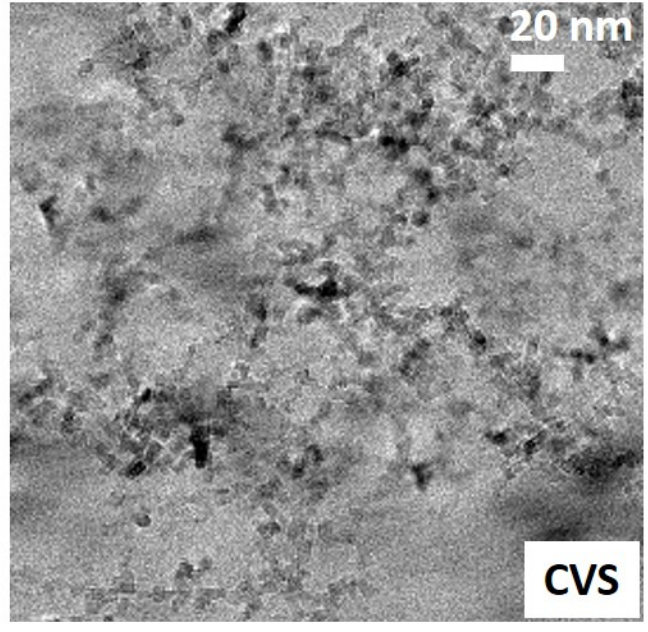
20 nm
CVS

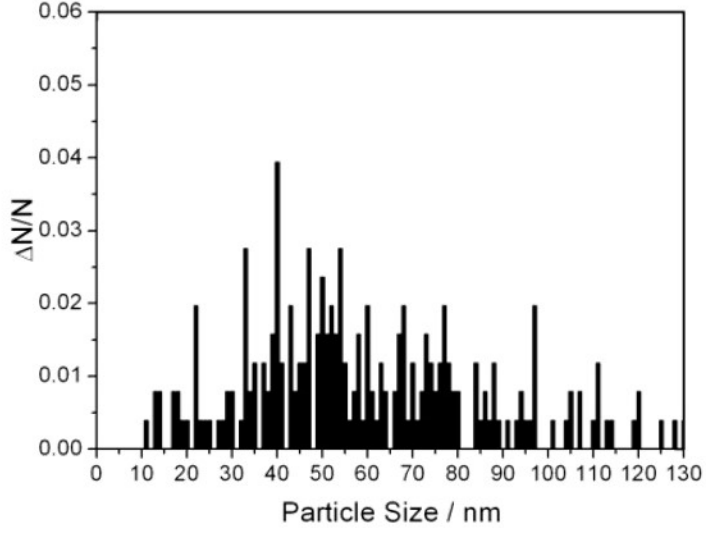
ΔN/N
Particle Size / nm

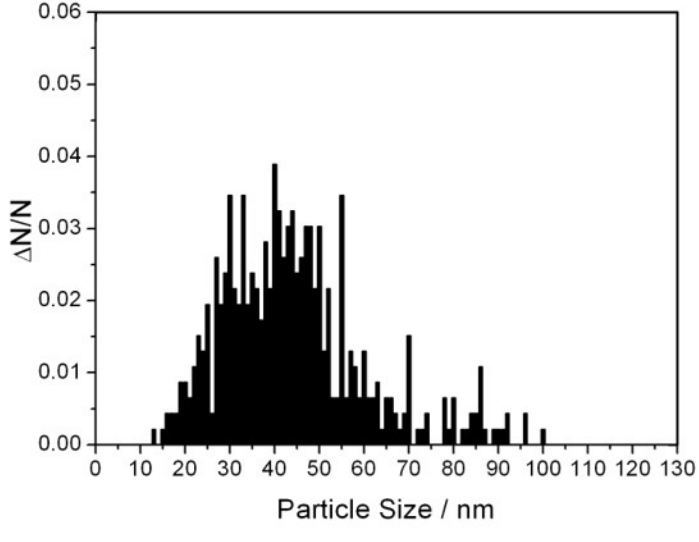
ΔN/N
Particle Size / nm

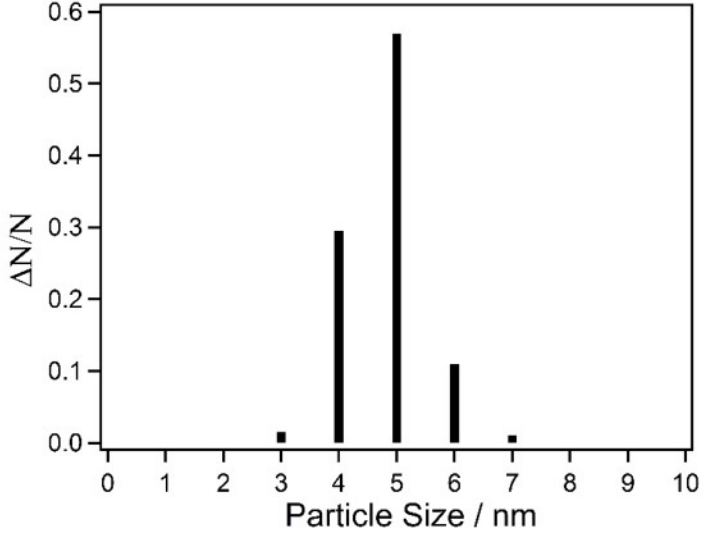
ΔN/N
Particle Size / nm

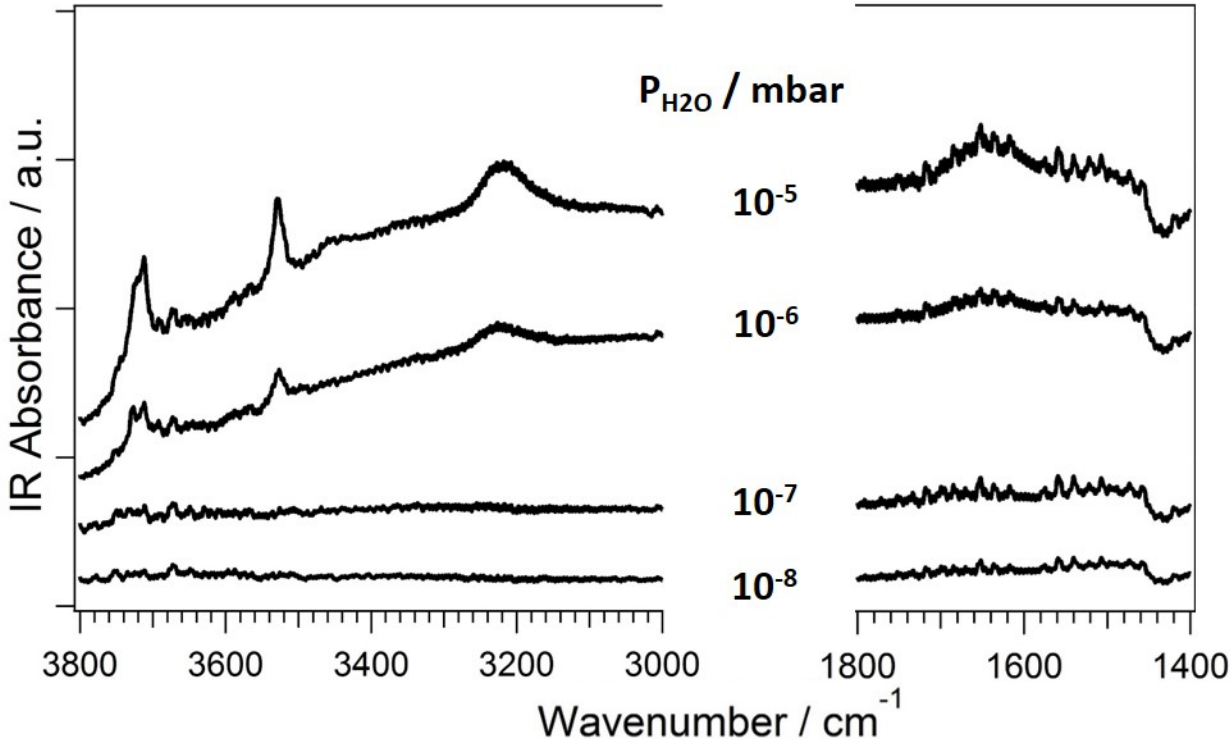
P$_{H2O}$ / mbar
10^{-5}
10^{-6}
10^{-7}
10^{-8}
IR Absorbance / a.u.
3800
3600
3400
3200
3000
1800
1600
1400
Wavenumber / cm^{-1}

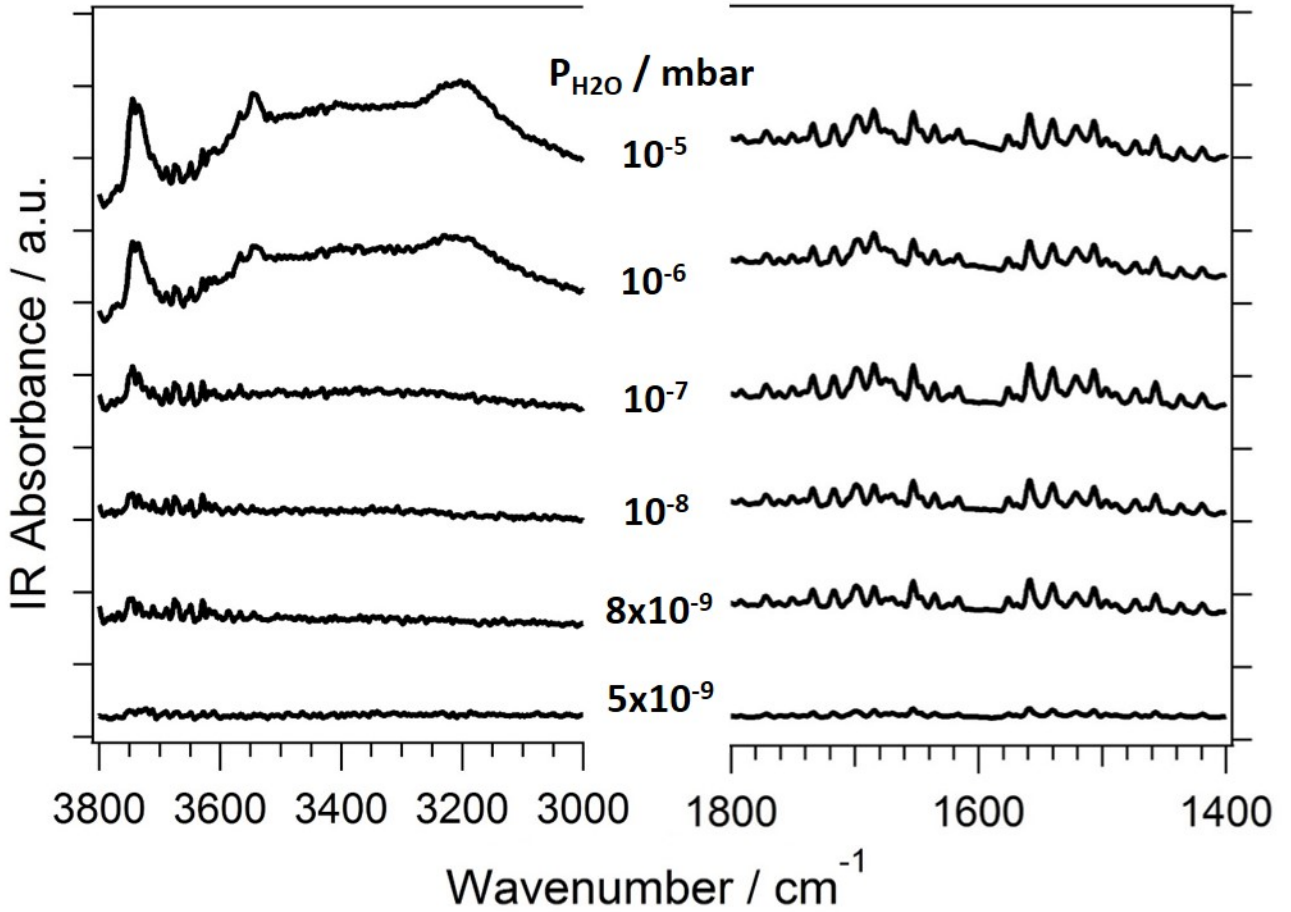
P$_{H2O}$ / mbar
10^{-5}
10^{-6}
10^{-7}
10^{-8}
8x10^{-9}
5x10^{-9}
IR Absorbance / a.u.
3800 3600 3400 3200 3000
1800 1600 1400
Wavenumber / cm^{-1}

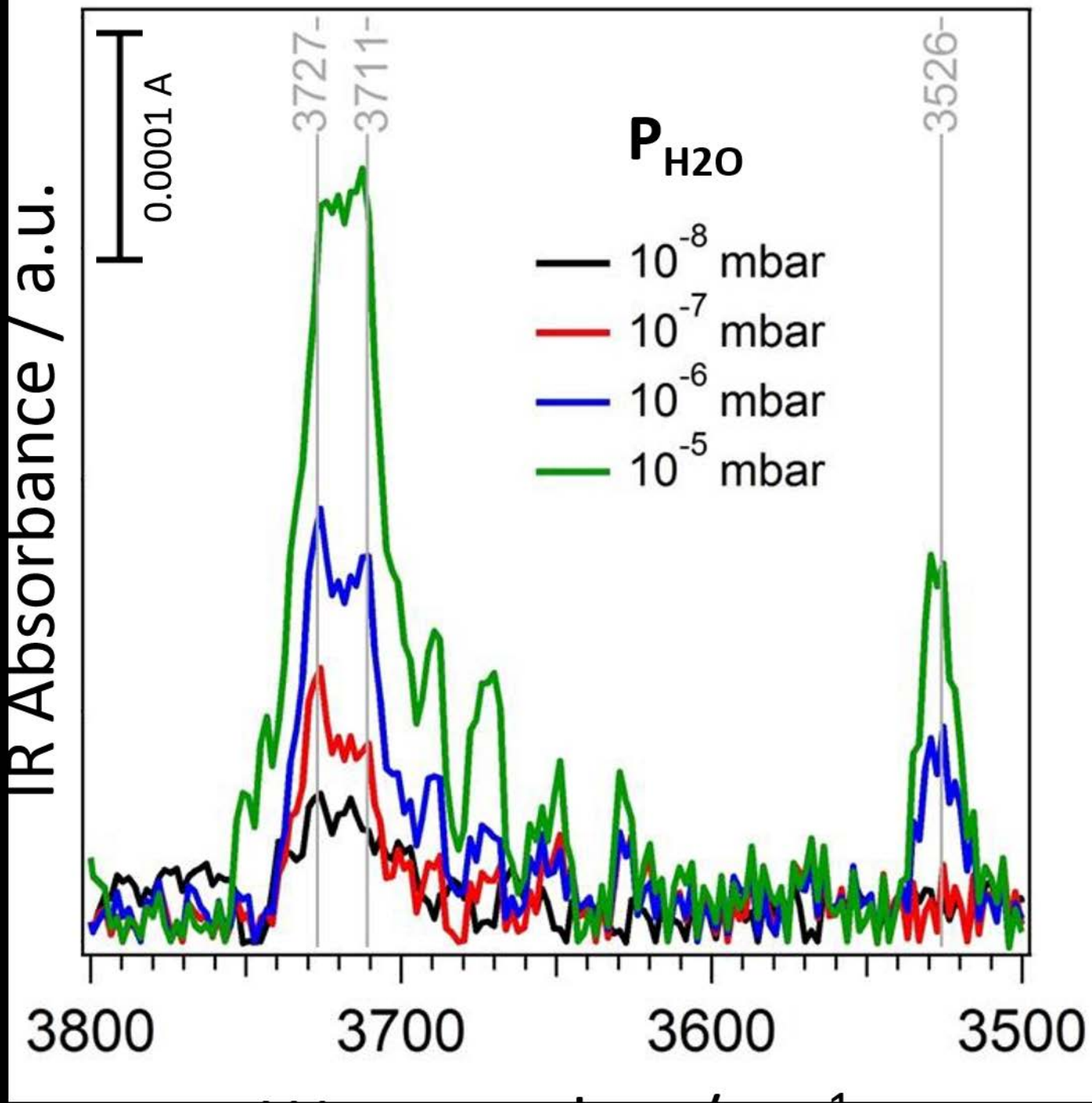
IR Absorbance / a.u.
0.0001 A
3727-
3711-
3526-
P_{H2O}
10^{-8} mbar
10^{-7} mbar
10^{-6} mbar
10^{-5} mbar
3800
3700
3600
3500

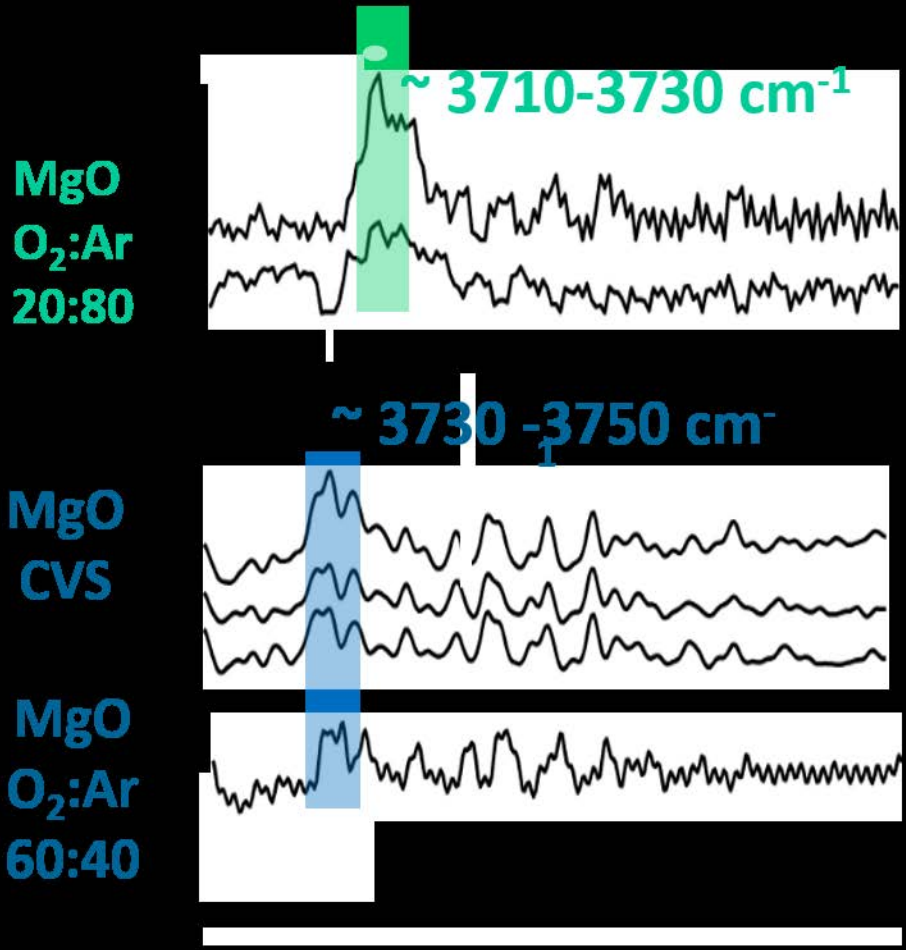
~ 3710-3730 cm-1
MgO
O2:Ar
20:80
~ 3730 -3750 cm-1
MgO
CVS
MgO
O2:Ar
60:40

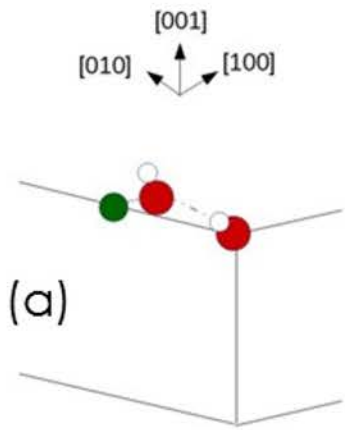

Corners

$O_{(1C)} - H$

$O_{(3C)} - H$

$O_{(1C)} - H$

$O_{(4C)} - H$

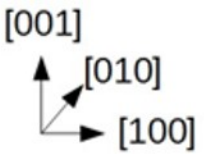

Isolated H_2O

O_{2C} – H 3750 cm^{-1}

O_{4C} – H 3290 cm^{-1}

Full coverage

O_{2C} – H 3760 cm^{-1}

O_{4C} – H 3510 cm^{-1}

(a)

<010> step

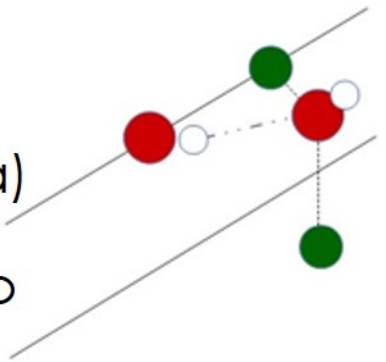

(b)

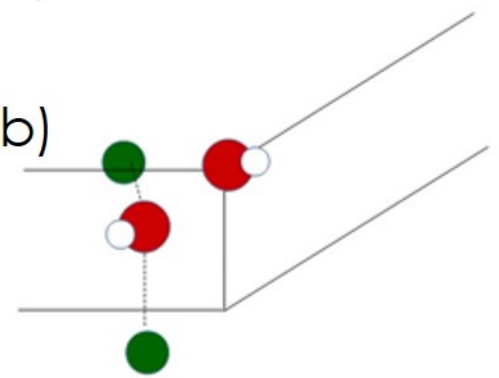

O_{2C} – H 3750 cm^{-1}

O_{3C} – H 3735 cm^{-1}

kinks @

<010> step

(c)

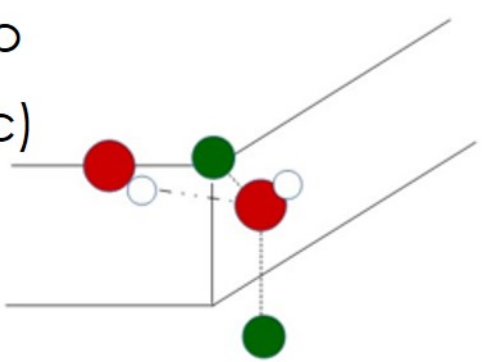

O_{2C} – H 3760 cm^{-1}

O_{4C} – H 3500 cm^{-1}